We are IntechOpen,
the world's leading publisher of Open Access books
Built by scientists, for scientists

6,900
Open access books available

186,000
International authors and editors

200M
Downloads

154
Countries delivered to

Our authors are among the

TOP 1%
most cited scientists

12.2%
Contributors from top 500 universities

BOOK CITATION INDEX
CLARIVATE ANALYTICS
INDEXED

WEB OF SCIENCE™

Selection of our books indexed in the Book Citation Index
in Web of Science™ Core Collection (BKCI)

Interested in publishing with us?
Contact book.department@intechopen.com

Spintronics Driven by Superconducting Proximity Effect

Guoxing Miao

Additional information is available at the end of the chapter

http://dx.doi.org/10.5772/59942

1. Introduction

In this chapter, we will discuss a few selected topics on the applications of superconducting proximity effect, and the related inverse proximity effect, in the field of spintronics. Superconducting proximity effect occurs when Cooper pairs from a superconductor propagate into the adjacent metallic systems and induce superconducting correlations in the otherwise non-superconducting materials. Due to the limited coherence length of Cooper pairs, this effect is confined to the very interface between the two materials and can be used as a method to trigger supercurrent flow, or to create particle-hole symmetry, in a wide range of devices. The inverse proximity effect can be viewed as the counteraction of the above-mentioned effect. Superconductivity in the original superconductor material inevitably weakens when it drives superconductivity into its neighbours; in addition, back flow of unpaired electrons and sometimes spin polarized electrons, will create more pair breaking within the superconductor and weaken it further. These effects can, however, be used as effective ways to control superconductivity through spin manipulations.

This chapter is organized in the following way. After a brief introduction on superconducting proximity effect and inverse proximity effects, we will continue our discussions from a few device points of view. 1. Proximity induced superconductivity in low dimensional electron systems, such as in the surface states of a 3D topological insulator and in the Rashba-split bands of a heavy metal/semiconductor nanowire. These form the most promising platforms that can host the elusive Majorana fermions for quantum computing applications. 2. Inverse proximity from multiple ferromagnetic neighbours can controllably turn superconductivity On and Off. The change in superconductivity states also leads to a large change in the device resistance, known as the superconducting spin valve effect.

i.   Superconducting proximity effect — the example of Majorana fermion creation

ii.   Inverse proximity on superconductors — the example of superconducting spin valves

2. Superconducting proximity effect — the example of Majorana fermion creation

The term superconducting proximity effect [1, 2], by default, refers to the leak-out of a superconductor's Cooper pair wave function into an otherwise non-superconducting material, and the generation of induced superconductivity in that material. This is a spontaneous process that occurs whenever the superconductor makes clean enough contact with a metallic system. Fig.1 illustrates the distribution of superconductor pairing potential Δ across the interface between a superconductor and a normal metal. Far away from the interface, Δ simply sits at the respective bulk values, being Δ_0 on the superconductor side and vanishing on the normal metal side. The proximity effect shows up clearly near the interface: Δ is weakened on the superconductor side but gradually emerges in the normal metal towards the interface. Naturally, the two systems have to be in atomic contact for such wave function overlap to happen effectively. The interface transparency is critical for the strength of the proximity, and is often characterized with an impedance parameter γ_B such that the interfacial transparency $T = \frac{1}{1+\gamma_B}$. The transparency captures the interfacial quality as well as the wave function matching between the materials. In Fig.1, a clear discontinuity is seen across the interface which indicates a less-than-perfect interfacial transparency. A cleaner interface means stronger proximity, which adds some quite stringent requirements to the materials' development.
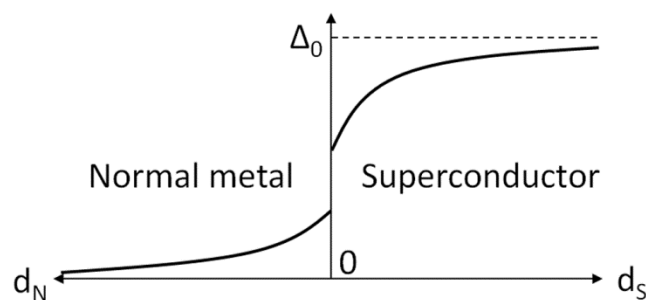

Figure 1. Evolution of the superconductor pairing potential Δ near an S/N interface. Δ_0 is the bulk pairing potential of the superconductor.

Such superconducting proximity effect is of particular interest to the spintronics community because it not only allows for spontaneously driving a non-superconducting material into superconductivity, but also enables actively pumping supercurrents over a pro-longed distance across a non-superconducting material. Their fundamental principles are the same: extension of the superconductor wave function into the non-superconducting material. Naturally, the proximity effect can propagate into a material as long as there are available electronic states near the Fermi level: i.e., a metallic material. There have been some quite important reports in the field demonstrating superconductor coupling through unconventional media: for example, the manifestation in 2D semiconductor electron gases [3, 4, 5] and topological insulator surface states [6, 7, 8]; the two-valley nature with

relativistic Dirac electrons of graphene [9]; the gate tunability when coupled to 1D carbon nanotubes [10, 11], as well as with 0D C_{60} molecules [12] and InAs quantum dots [13]; the flow of supercurrents through double-stranded DNA molecules [14]; and the conversion into spin triplet supercurrents in half-metals [15, 16].

Whereas the superconducting proximity effect can essentially drive any electron system into superconducting, we focus our attention on a very specific topic: generation of the long-sought-after Majorana fermions on superconductor platforms and application of these particles to topological quantum information processing [17]. A Majorana fermion, by definition, is a spin-1/2 particle identical to its own antiparticle, as opposed to a conventional Dirac fermion. Being its own antiparticle suggests that the particle has to be charge neutral as well. A superconductor's wavefunction has perfect electron-hole symmetry, making it an ideal platform for creating objects with similar properties. Other than being electrically charged, the quasiparticle excitations in a superconductor come really close to the Majorana fermions. Naturally, many of the proposals for creating Majorana fermions in solid-state systems involve superconductivity as one of the core ingredients. There are a number of ingenious device concepts for realizing Majorana fermions in a superconductor platform. The most practical route of synthesizing a localized Majorana fermion is to build on the platform of p-wave superconductors [18, 19] such as strontium ruthenate (Sr_2RuO_4): a spinless p_x+ip_y superconductor [20]. A p-wave superconductor's wavefunction is two-fold degenerate and has chirality on the angular momentum; it is therefore often termed the chiral p-wave state. It differs from the more conventional s-wave BCS superconductors and d-wave high-temperature superconductors in the sense that the electrons prefer to pair into spin-triplet configurations. Since ferromagnetism is observed in many closely related strontium ruthenate compounds (such as $SrRuO_3$), it is natural to consider the possibility of triplet pairing on these superconducting species. There has been compelling evidence confirming that Sr_2RuO_4 is indeed a p-wave superconductor [21]. This spontaneous time-reversal symmetry breaking ensures that the system is stable against magnetic impurity scattering, but not so much against normal elastic impurity scatterings, such as from non-magnetic defects, grain boundaries, or surfaces. As a result, it is very hard to obtain materials with a high enough quality for device purposes. With Sr_2RuO_4 as an example, while its T_C can reach as much as 1.5 K in the best-quality single crystals, it is practically non-superconducting in any of the thin films deposited so far [21], which is a significant obstacle for its potential application in the topological quantum computer architectures.

The superconductor proximity effect comes in as an experimentally feasible route to "simulate" a p-wave superconductor that can subsequently host Majorana modes on the resulting 2D platforms [22, 23]. Now that the particle-hole symmetry has already been guaranteed on the given platforms by the superconductivity induced from the superconducting proximity effect, what about the spinless nature of the p-wave superconductors? The signature we need to look for is the so-called helical Dirac spin state, as illustrated in Fig.2, which readily shows up on the surface of a 3D topological insulator [24]. A 3D topological insulator is a quantum spin Hall insulator with an inside that is insulating and a surface that is conducting [25]. Due

to the nontrivial topology of the material, its interface with a topologically trivial insulator, such as a normal insulator or vacuum, always has the conducting surface states present, which are strictly protected by the topological orders. We will not go into too much detail about topological insulator itself as it is not the focus of this article, except to point out that: a) the electron dispersion relation shows a helical spin texture — the electrons' spin orientation and momentum direction are tightly locked due to strong spin-orbit coupling; b) the dispersion is linear for the energy range we are interested in — known as the relativistic Dirac dispersion; and c) there is no energy gap and no spin degeneracy — a single band structure, different from a zero-gap semimetal or the spin and valley degenerate graphene. As the ingenious proposal from Fu and Kane [22] demonstrates, by coupling the helical surface states of a topological insulator with a conventional s-wave BCS superconductor through proximity effect, one can essentially simulate the properties of a p-wave superconductor and perform any subsequent operations with the composite states. Due to the two-dimensional nature of the topological surface states, the resultant "p-wave superconductor" is also two-dimensional. When a vortex nucleates on such a surface, it defines a non-superconducting region which essentially creates an "edge" on the surface localized to a tiny circle. A closed contour around this circle has a Berry phase shift of π due to the rotation of spin orientation around this circle. A Majorana zero mode is trapped within this vortex core, and can therefore be moved coherently when one physically moves this vortex around, as if it is a standalone physical particle. Once these localized, non-Abelian Majorana bound states are established, one can then perform the necessary braiding operation on them which covers all the quantum gates required for quantum information processing [17].
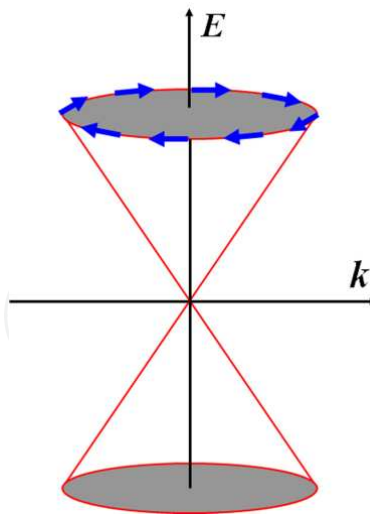

Figure 2. Electron energy dispersion with a helical spin texture similar to the surface states of a topological insulator. Blue arrows indicate the directions of the spins, and red cones indicate the linear dispersion near the Dirac point.

Though a topological insulator makes a convenient platform for creating a p-wave supercon-ductor and the subsequent Majorana fermions, the above proposal remains an experimental challenge mainly due to the difficulties associated with perfecting the topological materials

themselves, which requires significantly more effort along the road [24, 26, 27, 28]. Experi‐
mentalists have progressed remarkably further on a much more mature material platform: the
surface of a semiconductor with strong Rashba spin-orbit coupling. Evidence of Majorana
bound states has already been reported in this direction [29, 30, 31]. The basic idea here is to
also look for an electronic state that resembles the helical spin states as described above, and
the Rashba spin-orbit coupling, resulting from structural change at interfaces; this idea can
become a convenient solution to the problem. Fig.3 illustrates the effect of Rashba spin-orbit
coupling on a "free" electron band. Due to the relativistic effect, electrons moving in the
interfacial electric fields also experience effective magnetic fields on their rest frame. Forward-
moving electrons and backward-moving electrons see opposite in-plane effective magnetic
fields. In the forward-moving direction, the spin-"inward" electrons are lifted higher in energy
than the spin-"outward" electrons, and vice versa in the opposite-moving direction. Here the
inward and outward spin orientations are with respect to the paper of drawing, and which
spin configuration has lower energy is also determined by the Rashba field direction of that
interface. Note that the spins are still degenerate at the k=0 point where the spin-orbit coupling
vanishes, and it creates a crossing between the two bands. The dispersion relation is nearly
linear in k close to this crossing point. Fig.3 only depicts the situation of one-dimensional
electron motions (x-direction). Imagine that we are actually dealing with a two-dimensional
surface, and the k space extends in both x and y directions. This will revolve the spin-split
bands around the centre axis of k=0, and the crossing point evolves into a Dirac point under
the electrons' two-dimensional motion. Because the Rashba field is normal to the xy-plane
electron motion, the resulting effective magnetic fields — and therefore the principle spin
quantum axes —always lie within the xy-plane and transverse to the direction of motion. This
leads to a helical spin texture as depicted in Fig.3. Note that two helical spin-textured Fermi
surfaces exist in this structure and a perpendicular Zeeman field along z-direction is necessary
to open a gap at the Dirac point and remove the spin degeneracy from this system, eventually
rendering it spinless. With this construction of a helical spin state through Rashba spin-orbit
coupling, we can again proceed with superconducting proximity effect to simulate the
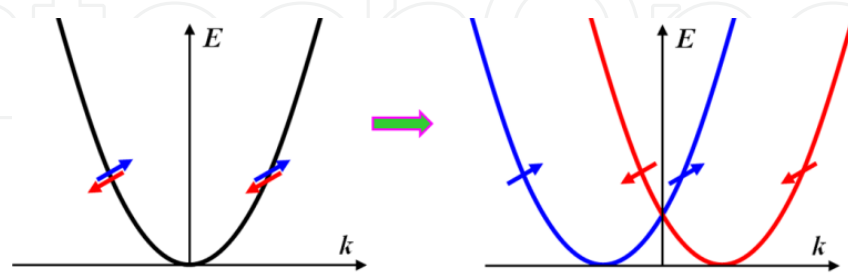properties of a p-wave superconductor.

Figure 3. Illustration of a Rashba type spin-orbit splitting. Left: a typical parabolic "free" electron band with two-fold
spin degeneracy. Right: In the presence of Rashba spin-orbit coupling, moving electrons feel an effective magnetic field
on their rest frame, and the two spin channels are therefore split in energy. The effect is linear with respect to the wave
vector *k*, and opposite for the two types of spins. Therefore, the Rashba spin-orbit coupling adds a linear component to
the quadratic function, creating a uniform shift of the parabolas from the origin but in opposite directions for the oppo‐
site spin channels.

The proposal from Das Sarma et al. [23] is based on a 2D semiconductor electron system governed by the following equation of motion,

$$H_0 = \frac{\hbar^2 p^2}{2m^*} - \mu + V_z \sigma_z + \alpha \left(\vec{\sigma} \times \vec{p} \right) \cdot \hat{z} \tag{1}$$

Here, m^*, μ, V_z, α, are the electrons' effective mass, the chemical potential, the out-of-plane Zeeman splitting, and the Rashba spin-orbit coupling strength, respectively. Without the Zeeman term, the band structure would look just like that in Fig.3: revolving around the centre axis, as described above. We can easily see that the Zeeman term has a negligible influence on the total wavefunction when $\vec{p}$ is large, but becomes dominant close to $\vec{p} = 0$ and opens up an energy gap right at the Dirac point, with the gap size $2V_z$ determined by the electrons' g-factor and the applied Zeeman field strength. This perpendicular Zeeman field is critical in this proposal for removing the spin degeneracy from the structure, leaving only one band present within the Zeeman gap. One does need to carefully tune the Fermi level of the system to within this gap to take advantage of this feature. The next ingredient is the superconducting proximity effect, which will induce superconductivity into the semiconductor's Rashba-split surface states. In order for the proximity effect to be effective, the semiconductor needs to be sufficiently conducting, in addition to possessing strong Rashba spin-orbit coupling. These requirements readily identify some of the heavy-element, low-gap semiconductors as the most promising choices, such as InSb or InAs. They tend to also have very large conduction electron g-factors, dozens of times larger than 2, making them even more ideal in applied magnetic fields. The superconductors, on the other hand, tend to have lower critical magnetic fields if the field direction is pointing out of the film plane, and in many cases the superconductivity will be completely destroyed by a field of a few Tesla. In order to induce appreciable Zeeman splitting, hopefully a few meV or higher, without suppressing the superconductivity, magnetic insulators are often used in these proposals to induce the necessary perpendicular Zeeman field. These materials are known to produce large exchange Zeeman fields onto adjacent free electrons, and are most effective on low-dimensional 2D or 1D electron systems [32]. The induced effective field can reach hundreds of Tesla with this approach. With exchange fields being short ranged, they have negligible influence on the superconductivity because the superconductor and the magnetic insulator are not in direct contact. Later, Alicea et al. [33] offered a clever twist on the above proposals by combining the Dresselhaus spin-orbit coupling, intrinsic to III-V semiconductors because of their crystallographic inversion asymmetry, and the Rashba spin-orbit coupling, due to the structural inversion asymmetry at interfaces, in a semiconductor quantum well structure with selected crystalline orientations. Now that the principle spin quantum axis no longer lies within the electrons' motion plane, a magnetic field with reasonable strength applied parallel to the plane surface, coupled with the relatively large g-factors in these semiconductors, can also open up an appreciable energy gap at the centre point, removing the spin degeneracy found there. Once the spinless platform is constructed, the next important practice is to tune the chemical potential of the system right to the middle of this gap through chemical doping or electric field gating. One can then place

a conventional s-wave superconductor on top, which induces superconductivity into the system through proximity effect. The induced superconducting correlation opens up another energy gap on the conduction electrons and the system becomes fully gapped. With all these ingredients in place, the system can be described with exactly the same Bogoliubov-de Gennes (BdG) equations as the topological p-wave superconductors, and Majorana bound states are expected to exist at vortex cores on this special platform.
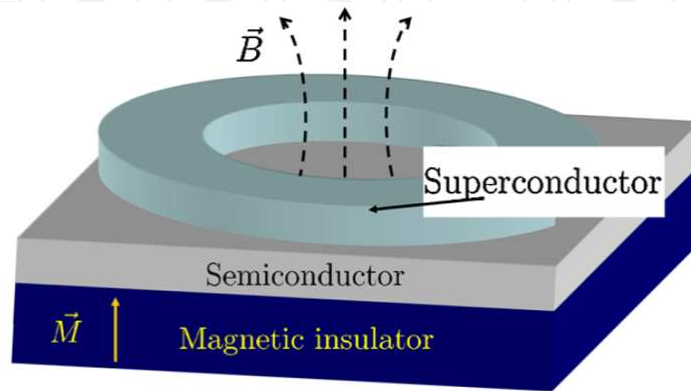

Figure 4. Majorana state bound to a vortex core on a heterostructure of a Rashba semiconductor platform, with both superconducting and magnetic proximity effects [23].

Another route of synthesizing Majorana fermions is to perform superconducting proximity on top of a heavy metal surface with strong Rashba spin-orbit coupling [34, 35]. The Rashba splitting tends to be much larger than in the semiconductor systems. Under the strong Rashba spin-orbit coupling, the metal's surface states also show two spin-split parabolas, with a crossing at k=0 similar to those shown in Fig.3. A perpendicular external magnetic field, or a perpendicular exchange field from magnetic insulators, will open up a Zeeman gap at the cross point, and an s-wave superconductor will induce superconductivity into the system through superconducting proximity effect. While the superconducting gap stays with the chemical potential of the system, one still needs to match the chemical potential to the middle of the Zeeman gap. Due to the abundance of carriers in the metallic systems, however, it is extremely difficult to move the chemical potential through electric field gating. Therefore, one has to carefully select a suitable electron system to begin with, with the crossing point of the surface states not too far from the metal's Fermi level. Fig.5 shows one such set-up. Tunnelling spectrum to the interface can reveal the existence of the desired, gapped Rashba surface states. Once the superconducting proximity effect kicks in, appearance of Majorana zero-energy modes can mediate resonant Andreev reflection between two leads, with perfect conductance of $2e^2/h$ independent on the coupling strength. As a comparison, conventional resonant Andreev reflection only shows the maximum conductance when the two coupling amplitudes are identical.

The construction of the p-wave-superconductor-like electron systems makes the search for Majorana fermions much more tangible for experimentalists. It is now possible to revisit Kitaev's initial concept of 1D wires hosting Majorana end modes [36], which has been subse-
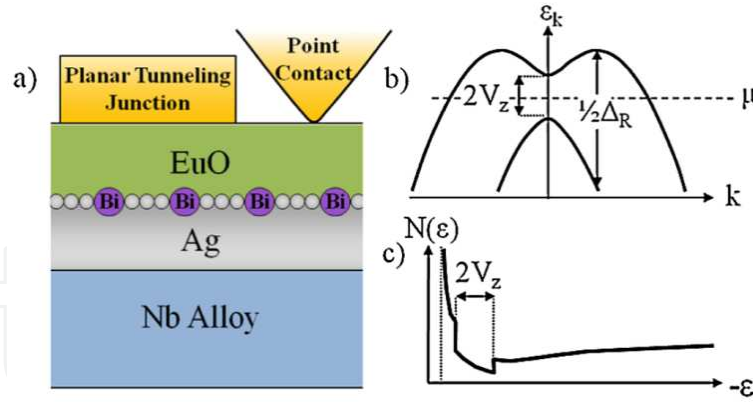
Figure 5. The proposed sample layout for the heavy-metal-based Majorana fermion creation [34]. (a) Ag(111) surface with 1/3 monolayer of Bi coverage in the ($\sqrt{3}\times\sqrt{3}$) R30° reconstruction. Superconducting proximity from an s-wave superconductor (Nb alloy), and magnetic proximity from a magnetic insulator (EuO), together create a topological superconductor channel on the system. (b) Electrons confined on the metal surface experience strong Rashba spin-orbit coupling and form two parabolas crossing at k=0. The gap of $2V_z$ comes from the exchange fields from EuO, and the chemical potential μ of the system needs to be tuned to the mid-gap. (c) Potential verification of the surface states through tunnelling spectrum, where one should see a dip corresponding to the opening of the exchange gap and a van Hove singularity corresponding to the very top of the Rashba bands.

quently extended onto semiconductor nanowire platforms coupled with strong superconducting proximity effect [37, 38, 39]. The two ends of a 1D wire form a protected pair of Majorana fermions. This is analogous to a vortex on a 2D topological superconductor, which is also a boundary of the 2D platform but a physically moveable entity. To create a 1D p-wave superconductor wire, one can start with a 1D semiconductor wire and drive it into superconductivity with superconducting proximity effect. The regions surrounding the nanowire are just topologically trivial superconductors/insulators, leaving the enclosed topological superconductor nanowire intact. One can also start with the constructed 2D p-wave superconductor platforms as described earlier, and use selected electric and magnetic manipulation to suppress or flip the polarity of the topological superconductivity in order to define the desired 1D nanowire region with a distinct topology. Specifically, magnetic insulators can exert very strong interfacial exchange fields onto the desired 2D platforms, and can therefore be used as a local control to open and close the Zeeman gap of the system without much adverse influence on the superconductor system. Electric field manipulation from gate electrodes allows for local and active tuning of chemical potentials in the system. The topologically nontrivial superconductor state is enabled when the chemical potential is tuned into the mid gap, and will be destroyed when it is too far off. Therefore, we see that we can conveniently perform the fusion and braiding operations on the Majorana end modes with controlled gating on the 1D wire networks [39]. Similar manipulations can also be achieved on 2D platforms by controllably moving the vortices. Quantum information is stored non-locally on these non-Abelian systems and therefore is largely immune to any local perturbations, as long as the topology of the above systems remains protected by the superconducting and exchange gaps. These properties ensure that topological quantum computing on these solid-state platforms is inherently error-tolerant. We will not discuss in this article the details of braiding operations for topological quantum information processing, except to point out that quantum braids cover all the

necessary quantum gates required for quantum computing. One can refer to the original article by Kitaev et al. [17] for an accurate account for topological quantum computation with non-Abelian anyons.

There have been a number of reports about successfully observing the signatures of Majorana fermions along the route of the proposed proximity-driven platforms [29,30,31, 40, 41, 42]. Semiconductors offer the most opportunities so far because of their maturity in technology. The first convincing report [29] was based on InSb nanowires with strong spin-orbit coupling and a very large g-factor (g≈50), and the device layout is shown in Fig.6. The nanowire portion under the superconductor is the region of interest, where the superconducting proximity effect drives this nanowire region into superconducting. Note that the superconductor only covers half of the wire in order that the electric fields coming from the buried gate electrodes are not completely screened. This practice is very important to ensure that the chemical potential of this portion of wire can be tuned into the middle of the Zeeman-split gap with controlled gating. The semiconductor nanowire with strong Rashba spin-orbit coupling can be treated as a quasi-1D electron system, and its dispersion relation is essentially the same as that illustrated in Fig.3's right-hand panel, with two Rashba-spin-split parabolas in zero magnetic fields. In the nanowire geometry, one can find that when the applied magnetic field is along the wire direction, a Zeeman energy gap opens up at the Dirac point of the dispersion curve. The above actions ensure that Majorana bound states will emerge at the ends of the wire when the topological superconductor phase disappears and the normal gapped semiconductor/superconductor phase emerges. A quantum mechanical tunnelling measurement on this Majorana mode confirmed that it is bound strictly at zero energy throughout the field range in which it is supported. It emerges when the field applied along the wire opens up the Zeeman gap, and disappears when the field becomes too strong and destroys the topological super-conductor phase. The behaviour is distinctly different from other phenomena such as Andreev reflection and Kondo effect, and is therefore widely accepted as the first observation of Majorana bound states in solid-state systems. The bound state vanishes under elevated temperatures, because thermal excitations start to overcome the gap protections. Strictly speaking, a semiconductor nanowire is not exactly a 1D electron system, and there are multiple transverse subbands due to the finite width. The above 1D wire theory was expanded to the more general multichannel situations [34, 43], and the protected Majorana modes exist in the quasi-1D wires as long as there are only an odd number of bands crossing the Fermi level and the wire is not substantially wider than the superconducting coherence length. These conditions are both satisfied in this experiment. The magnetic field was applied along the wire direction in this experiment, and a magnetic field perpendicular to the device plane (out-of-the-page) is no longer a suitable choice. The circular geometry of the nanowires leads to a circular distribution of the Rashba electric fields, and for some parts of the wire surface the applied magnetic field would be aligned parallel to the wire surface and perpendicular to the wire direction. Magnetic field in such a configuration is only able to shift the Dirac point a little bit in energy and momentum, but is not able to open up the desired exchange gap. Therefore, some parts of the wire would remain gapless if a perpendicular-to-the-device-plane magnetic field is chosen.
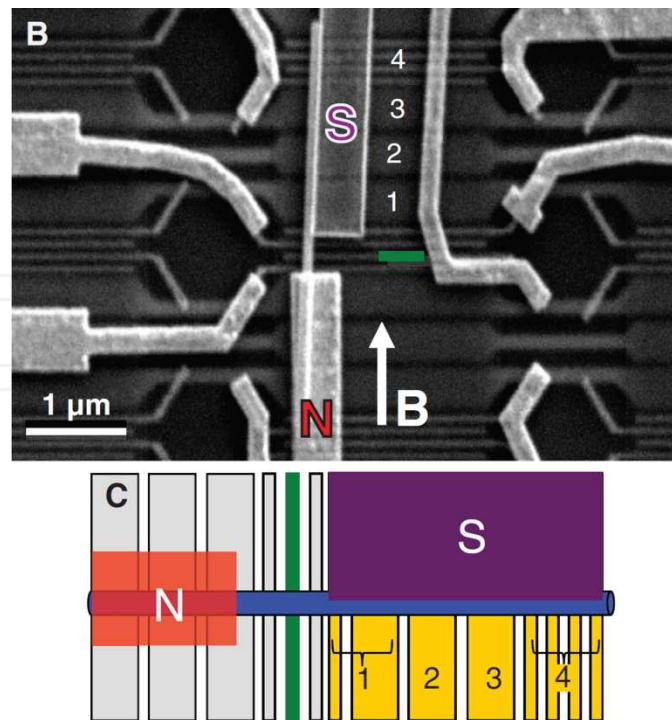
Figure 6. Device layout for the experimental evidence of Majorana fermion in a solid-state system [29]. The electrodes seen on the background, numbered 1, 2, 3, 4, etc., are the gate electrodes, separated from the nanowire and top electrodes by Si_3N_4 dielectrics. The nanowire is in contact with a normal metal (N) on one end, and a superconductor (S) on the other. The gate electrode labelled in dark green is the one used to create a tunnel barrier between the two sides of the nanowire. This effectively forms a S-NW-N tunnel junction for spectroscopy measurement. The nanowire region covered under the superconductor would have proximity-induced superconductivity in it, and a Majorana bound state is therefore trapped at the very edge of the superconductor region when the topology changes. It shows up as a zero-bias peak on the tunnel spectroscopy when a suitable magnetic field is applied along the wire direction.

3. Inverse proximity on superconductors — The example of superconducting spin valves

As we have described above, the superconducting proximity effect describes the superconductor's wavefunction propagating into non-superconducting materials and inducing superconducting paring in there. Because of the leak-out of paired electrons, and the influx of unpaired electrons, the proximity effect would naturally generate a counter effect that weakens the superconductor itself. This is known as the inverse proximity effect. We will only focus our attention on a specific aspect of it — inverse proximity from ferromagnetic materials. The presence of spin information in the ferromagnets allows for spintronic manipulation on the superconductor system. For a detailed review on superconducting proximity with ferromagnets, please see the thorough review articles by Buzdin and Bergeret et al. [44, 45]. Here we proceed to demonstrate the inverse proximity effect from ferromagnets by illustrating with superconducting spin valve devices that can essentially turn the superconductivity On and Off through spin manipulations.

The propagation of superconductor wavefunction in a ferromagnetic metal is qualitatively different from that in a normal metal. This originates from the mutual incompatibility between a BCS superconductor, in which opposite spins pair up into Cooper pairs, and a ferromagnet, in which spins prefer to align parallel to each other to minimize the exchange energy. The presence of magnetic species in or near a superconductor material could be a drag if one wants to maximize the performance of the superconductor, because magnetic interactions break time reversal symmetry and become a strong source of Cooper pair breaking. We can, however, achieve desired controllability on the superconductor devices through manipulating the proximity-coupled magnetic systems. Fig.7 illustrates the propagation of superconducting wavefunction into a ferromagnetic metal. We note that instead of a simple exponential decay as in the normal metal/superconductor situation (Fig.1), the superconducting order parameter picks up a fast oscillatory behaviour. This can be qualitatively understood by considering the two electrons of a Cooper pair with opposite spins sitting inside an exchange field. One of the electrons, with its spin aligned along the exchange field direction, has its kinetic energy lowered by δE, while the opposite electron sees an increase in its kinetic energy by δE in the exchange field. Therefore, they start to propagate with different wavevector k, and the Cooper pair as a whole no longer has zero net momentum as it used to when it was inside the superconductor. For an electron near the Fermi level of a parabolic band, the kinetic energy is quadratic to the wavevector k and an increase (or decrease) in the kinetic energy by δE leads to a change in the wavevector by $\delta E/\hbar v_F$, where v_F is the Fermi velocity. The Cooper pair now gains a centre-of-mass momentum of $2\delta E/v_F$, and therefore the order parameter of the Cooper pairs will oscillate in space with a period of $hv_F/2\delta E$. This roughly describes the system in the clean limit. For the dirty limit of a diffusive system, the Cooper pair motion can be described well with the Usadel equation [46]. Under the assumption that the exchange energy is much larger than the pairing energy, which is true for most ferromagnets relative to superconductors, the pair wave function can be solved and has a form of $\Delta \exp\left(-\frac{x}{\xi_f}\right)\cos(\frac{x}{\xi_f})$ [44], i.e., an oscillatory function with exponential damping. In this special situation, the decay length and the oscillation period coincide (but they do not have to in more general situations). Here, $\xi_f = \sqrt{D_f/\delta E}$, $D_f = \frac{1}{3}v_F l$ is the diffusion coefficient and l is the electrons' mean-free-path in the ferromagnet. The oscillatory behaviour of the pair wave function adds an oscillatory dependence to the structure's overall critical temperature [47] when the ferromagnet layer thickness is comparable or longer than the pair oscillating period ξ_F. This has been verified in various superconductor-ferromagnet bilayer structures [48, 49, 50, 51]. One can readily see that when the ferromagnet layer thickness is equal to $\pi\xi_F$, the wavefunction has a phase shift of π across the ferromagnet layer, and the superconductivity is therefore weakened. As the ferromagnet increases in thickness, the phase oscillates back and forth and the system shows an oscillatory, non-monotonic behaviour in the critical temperature. The parameter ξ_F can be approximately read out from the oscillation period of T_C. The oscillatory behaviour of the pair wavefunction shows up not only in the phases, but also in the electron density of states inside the ferromagnets. At certain distance away from the interface, the density of states can even become larger than the normal value in the absence of superconducting proximity [52].
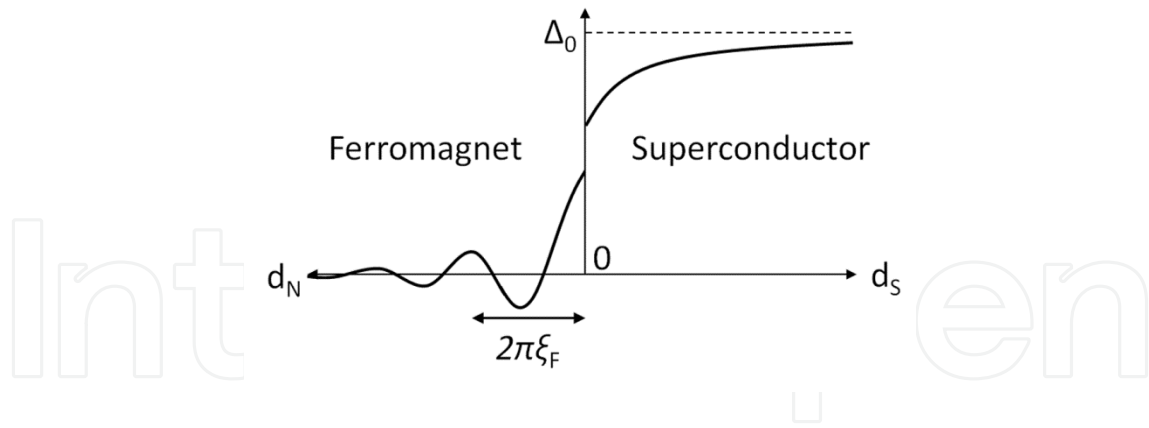
Figure 7. Evolution of the superconductor pairing potential near a S/F interface. The pairing potential inside the ferromagnet shows a strong oscillatory and damping behaviour due to the large internal exchange field. ξ_F characterizes the superconducting correlation oscillation length as well as the correlation decay length within a strong ferromagnet, where the exchange energy δE far exceeds the pairing potential Δ.

Though it is not immediately clear, the above discussions already imply that superconductivity within the superconductor itself will also be significantly weakened in the presence of a strong ferromagnet. A critical difference of the proximity with a strong ferromagnet, compared to that with a normal metal, is the extremely short decay length of the pairing potential. By connecting the superconducting wavefunction across the interface, one can already see that the steep slope of the pairing potential on the ferromagnet side influences that on the superconductor side and pulls the whole pairing potential profile downward. The exact boundary condition matching is subject to the interfacial transparency and the respective diffusion coefficients. A stronger ferromagnet creates stronger exchange interaction and shorter ξ_F: therefore, stronger suppression to the superconductivity. Now we can consider constructing a sandwich of ferromagnet/superconductor/ferromagnet: i.e., a superconducting spin valve structure [53, 54]. Although the two ferromagnet layers will both strongly suppress superconductivity in the sandwiched middle layer, we can try to cancel out their influence through spin manipulation. Recall that when one of the ferromagnet layers is placed on top of the superconductor, strong suppression of superconductivity is present. If we place the second ferromagnet layer with the same spin polarity, the inverse proximity effects coming from both ferromagnets strengthen each other and suppress superconductivity even more. This spin-parallel configuration ensures that the wavefunction over the whole structure is symmetric with respect to the film centre (mid-plane of the superconductor). We can conceptually fold the wavefunction in the middle and it becomes identical to that of a bilayer situation. Because the equivalent thickness of the superconductor layer is only half of its actual thickness, the layer suffers even stronger suppression from the inverse proximity effect. If we instead place the second ferromagnet with an opposite spin polarity relative to the first one, i.e., configuring the system into a spin-antiparallel state, the proximity effects from the two ferromagnets differ precisely by a phase of π and will largely cancel each other out. Superconductivity is therefore restored in this configuration.

We now use an epitaxial pristine structure of Fe/V/Fe as an example to illustrate the above mentioned superconducting spin valve effect [51]. The structure was deposited with molecular

beam epitaxy (MBE) onto MgO-buffered Si(100) substrates. X-ray diffraction verified the epitaxy of the films showing clear four-fold symmetry in the off-axis diffraction patterns. The quality of the films and interfaces can be verified with the critical temperature T_C and upper critical field H_{C2} measurements on V single layer films and Fe/V bilayer films. Fig.8 (a) shows that T_C varies linearly with respect to the inverse film thickness. Such dependence indicates clearly that there exists a superconducting "dead" layer on the film surface due to the lowering of electron density and weakening of phonon coupling there [55]. This surface layer is superconductingly inactive, and amounts to about 1 atomic layer (0.18 nm) on the pure V films (interfaced with MgO on both sides), confirming the superior quality of these films. On the other hand, the series of bilayer samples of V with proximity to 6 nm Fe show a significantly steeper slope, corresponding to a much thicker inactive layer of 13.5 nm. For V of the same thickness, presence of Fe pulls T_C much lower than MgO does in pure V films. This is a clear manifestation of the above-described inverse superconducting proximity effect: the presence of a ferromagnet strongly suppresses superconductivity in the adjacent superconductor. Fig. 8 (b) shows the upper critical fields of the set of films with 30 nm V. The addition of proximity from Fe again significantly suppresses superconductivity. The linear dependence of H_{C2} square with respect to temperature is an indication of two-dimensional superconductivity behaviour, which follows $H_{C2}(T) = H_{C2}(0)(1 - \frac{T}{T_C})^{1/2}$ [56]. From the determined slope of the plot, we can identify the superconducting coherence length ξ_S, being about 8.2 nm for the 30 nm V films. It is interesting to note that the slope does not change when the proximity effect from Fe kicks in, indicating that no change happens to the Cooper pair correlations. This is quite expected because the proximity effect and inverse proximity effect do not modify the pairing mechanisms within the superconductor, and the addition of a few nm metals has little influence on the electrons' mean-free-paths either. Fig.8 (c) shows the most important aspects of the inverse superconducting proximity effect: the quick oscillation and damping of T_C with thickness. As we have described earlier, T_C oscillates with the ferromagnetic layer thickness because of the Cooper pairs' phase oscillation inside an exchange field. We can roughly estimate the superconducting correlation length inside the ferromagnet ξ_F to be about 1 nm. We can also clearly see that the superconductivity suppression from inverse proximity effect is quite dramatic: with a few monolayers of Fe overlayer, the critical temperature already drops from the original value of over 5K to only slightly above 3K. The oscillation quickly damps out after several ξ_F, when the Cooper pair wavefunction is almost fully suppressed. After the first few nm, further increase of the ferromagnetic layer thickness does not continue to influence the overall wavefunction. On the other hand, we notice that T_C does not really drop to zero before recovering, as we have depicted before. This actually is also a consequence of the fast damping behaviour which significantly limits the transparency of the Cooper pairs into the ferromagnet. Beyond the first few nm, the remaining portion of the ferromagnet has no significant further contribution to the T_C suppression. In addition, because the measurement of T_C is over the whole structure, the region of the superconductor far away from the interface essentially retains the original superconductivity strength, and renders the whole structure superconducting under conventional DC measurements. Detailed calculations on T_C of such ferromagnet/superconductor bilayer structures confirm that the oscillation indeed quickly reaches a saturation value after the ferromagnet thickness increases beyond the first few oscillations [57].
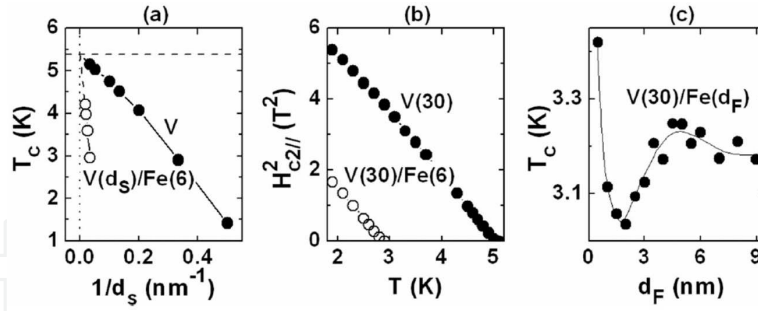
Figure 8. Critical temperature T_C and upper critical field H_{C2} for epitaxial V and Fe/V films [51]. (a) T_C as a function of inverse V layer thickness; (b) H_{C2} square as a function of temperature; (c) T_C damping and oscillation with respect to the Fe layer thickness, the solid line is provided as a guide for the eye. ξ_F can be estimated to be about 1 nm.

Next, we consider the magnetoresistance of these superconducting spin valves. The structure is fully epitaxial, with high interfacial quality. In order to magnetically separate the two Fe layers, a CoO antiferromagnetic layer was introduced above the top Fe layer, which exerts exchange bias [58] on the top Fe layer and essentially pins the magnetization of this layer to a chosen direction. When the applied magnetic field only sweeps in a range not exceeding the exchange bias pinning strength, one can only observe magnetic switching of the "free" layer, which is the bottom Fe layer in this structure. Fig.9 (a) shows the magnetoresistance results across temperatures close to T_C. When the magnetic field varies, clear resistance high and low states are observed, indicating that the structure toggles between the non-superconducting and superconducting states. In the spin-parallel configuration, the inverse proximity effects from both ferromagnet layers strengthen each other and strongly suppress superconductivity of the sandwiched V layer, leading to the high-resistance, non-superconducting state; in the spin-antiparallel configuration, the inverse proximity effects largely cancel each other out and the system returns to the low resistance, superconducting state. For certain temperatures the ratio between the normal resistance and the superconducting resistance is essentially infinite, making the magnetoresistance ratio essentially infinite. The effect is only pronounced in a very narrow temperature window close to T_C, because this is when the superconductivity is already quite weakened by thermal energy, and slight perturbations from the environment (such as from the inverse proximity effects) can readily drive the system in and out of its superconducting state.

Fig.9 (b) shows T_C determined for the two spin configurations. Clearly, spin-parallel state has weaker superconductivity and lower T_C, while spin-antiparallel state has stronger superconductivity and higher T_C. In the temperature range between these two T_C, a large resistance difference exists between the two states leading to the large magnetoresistance described above. The superconducting spin valve effect relies on the fact that the two ferromagnet layers are effectively coupled to each other through the superconductor. Therefore, the effect decreases as the superconductor layer thickness increases, and essentially drops to zero when the superconductor layer is much thicker than the superconducting coherence length ξ_S of about 8 nm in this system. On the other hand, if the superconductor layer is too thin, its superconductivity would be fully suppressed by the Fe layers and the superconducting spin
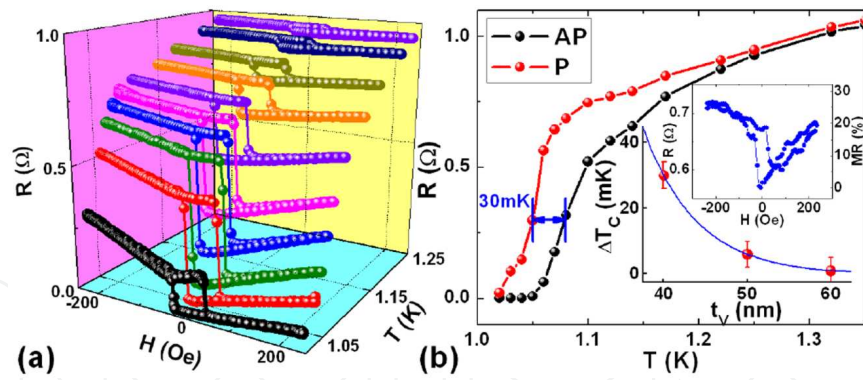
Figure 9. Measured superconducting spin valve effect in the epitaxial Fe/V/Fe structure [51]. (a) Device resistance as a function of applied magnetic field H and temperature T. A large magnetoresistance is associated with the switching of the free Fe layer in the temperature range close to T_C. (b) Resistance as a function of temperature for the structure in its spin-parallel (P) and spin-antiparallel (AP) configurations. There is a clear offset of 30mK between their corresponding T_C's. Inset: T_C offset as a function of the V layer thickness, and an example of a magnetoresistance curve for the sample with 50 nm V.

valve effect is also no longer achievable. The T_C shift as seen in Fig.9 (b) is clear indication of the operation temperature range of this effect, which is, however, limited to only tens of mK across many different systems [59, 60, 61, 62,51]. Improving interfacial transparency is the key for further improving the performance of these devices. Fig.10 shows the calculated variation of the P and AP T_C's with the change of the interfacial transparency [53]. The curves with the highest transparency (solid lines, T_F=25) clearly show a region with very large T_C shift. For example, around d_F/ξ_F=0.4, T_C of the AP state is around half the bulk value while that of the P state is fully suppressed. For samples of this structure, infinite magnetoresistance would show up for any temperatures below half the bulk T_C, making it a practically usable device for turning the superconductivity On and Off. As a comparison, for the curves corresponding to the lowest interfacial transparency, T_F = 1, the T_C difference between P and AP states is very small throughout all the d_F choices. This is easy to understand because poor interface transparency breaks up the correlation between the superconductor and the ferromagnets: therefore, the correlation between the two ferromagnets also vanishes. The two ferromagnets do not feel much influence from each other and the P and AP configurations make little difference. Although a weak superconducting spin valve effect is still present, the resultant magnetoresistance is very small and there is no truly On and Off tuning of superconductivity, making it less useful in practice.

We next examine a special type of superconducting spin valve, where the ferromagnet layers are not metallic but insulating [63]. The above described inverse superconducting proximity mechanism does not apply because the Cooper pair wavefunction cannot penetrate into the insulators. The inverse proximity happens due to the interfacial exchange interactions from the localized moments of the magnetic insulator, which exert a large effective Zeeman field onto the superconductor and can also suppress the superconductivity [32]. The interaction between the magnetic insulator and the carriers in the superconductor is through indirect exchange interaction, where the free electrons communicate with multiple localized magnetic moments of the magnetic insulator, and become spin-polarized in the process. This behaves
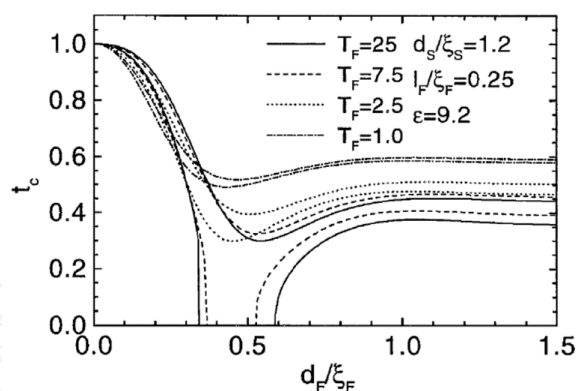
Figure 10. Expected T_C shift in superconducting spin valves when the interface transparency is varied [53]. Here d_S and d_F are the superconductor and ferromagnet layer thicknesses, l_F is the electron mean-free-path in the ferromagnet, ξ_S and ξ_F are the superconducting correlation lengths in the superconductor and ferromagnet, and ε is a parameter depending on the properties of both the superconductor and the ferromagnet, getting smaller with stronger ferromagnets. Two curves are shown for each choice of interfacial transparency, with the upper curve corresponding to the AP state and the lower one to the P state.

as an effective Zeeman field on the electron system and favours one type of spins over the other, therefore counteracts the tendency of Cooper pairing and suppresses superconductivity. Now that the magnetism-superconductivity interaction is established, it is again possible to use spin manipulations to control superconductivity in a sandwich structure [64]. The magnetic insulator material used in this study was EuS, which has been shown to generate exchange fields as large as a few Tesla on thin superconducting Al films [65, 66]. Under this effective Zeeman field on the conduction electrons, Cooper paring in the superconductor becomes less stable and superconductivity is thus weakened accordingly. A second magnetic insulator layer, when configured with its magnetic orientation opposite to the first one, will serve to cancel the exchange fields from the first one, provided that the electrons' mean-free-paths are long enough relative to the superconductor layer thickness such that the Zeeman fields from one side can propagate across the whole superconductor layer and influence the other side. As a result, we again recover a spin valve performance: when the two magnetic insulators are aligned parallel to each other, their exchange fields stack up and destroy the superconductivity in the system; when they are aligned antiparallel to each other, their effects cancel and the system goes back to the superconducting state. Experimentally, toggling the superconductivity On and Off leads to a very large magnetoresistance response, as shown in Fig.11. Here the system is in the spin-parallel state (finite resistance, non-superconducting state) when the external field is large and both EuS layers are saturated in the same direction; and in the spin-antiparallel state (zero resistance, superconducting state) when the external field is tuned between the magnetic switching fields of the two EuS layers, such that one of the layers flips while the other does not. Similar to the superconducting spin valves with magnetic metals, this effect only shows up in a very narrow temperature window close to T_C, when the superconductivity is already very weak to begin with. Though this effect appears very similar to the previously described superconducting spin valve effect, there is one critical difference: in this structure, there are negligible superconducting proximity and inverse proximity effects because of the insulating nature of the ferromagnets. The observed magnetic

tuning of superconductivity is in fact a result of the propagation of magnetic exchange interaction into the superconductor — the magnetic proximity effect, which is especially pronounced with magnetic insulators [32]. As a result, the system is described with the Cooper pairs feeling the average exchange fields *inside the superconductor* rather than with Cooper pairs feeling the exchange fields *inside the ferromagnets*.
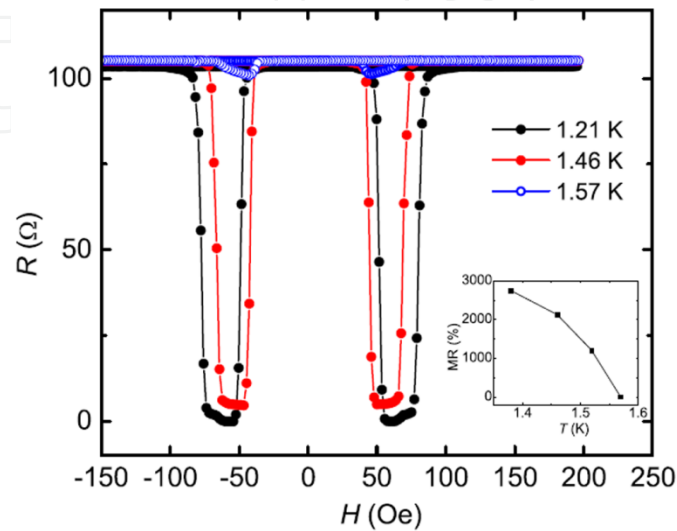

Figure 11. Superconducting spin valve effect in a magnetic insulator/superconductor/magnetic insulator sandwich structure (EuS/Al/EuS) [64]. Inset shows the variation of magnetoresistance ratio over the temperatures close to T_C.

4. Summary

In summary, we have used a few very specific examples (the creation of Majorana fermions on 2D surface states and the superconducting spin valves with ferromagnets) to illustrate the application of superconducting proximity and inverse proximity effects in spintronics. These examples can be viewed as passive devices of superconducting proximity/inverse proximity. One can also use active pumping of Cooper pairs to drive supercurrents into non-superconducting materials, which is yet another manifestation of the superconducting proximity effect and can induce superconducting Josephson coupling on many spintronics platforms, such as graphene and topological insulators. The Josephson effect will be covered in other chapters of this book and we will not discuss it in this chapter. Overall, we see that the superconducting proximity and inverse proximity effects are convenient approaches to couple superconductivity with many other types of spin systems, and allow us to create hybrid devices that can benefit from these very distinct spin states: superconductivity, magnetism, and topological quantum spin Hall state. Such manipulation of superconductivity offers important new routes for information storage and processing, and rapid advances are expected to happen in these directions taking information processing to the quantum level. We, as well as many other groups in the world, are actively working toward such goals.

Acknowledgements

Author details

Guoxing Miao[*]

Address all correspondence to: guo-xing.miao@uwaterloo.ca

Institute for Quantum Computing and Electrical and Computer Engineering, University of Waterloo, Waterloo ON, Canada

References

[1]   Meissner H, Superconductivity of Contacts with Interposed Barriers, Phys. Rev. 1960; 117: 672.

[2]   de Gennes P G, Boundary Effects in Superconductors, Rev. Mod. Phys. 1964; 36: 225.

[3]   Takayanagi H, Kawakami T, Superconducting Proximity Effect in the Native Inversion Layer on InAs, Phys. Rev. Lett. 1985; 54: 2449.

[4]   Nitta J, Akazaki T, Takayanagi H, Arai K, Transport Properties in an InAs-inserted-channel In0.52Al0.48As / In0.53Ga0.47As Heterostructure Coupled Superconducting Junction, Phys. Rev. B 1992; 46: 14286(R).

[5]   Nguyen C, Kroemer H, Hu E L, Anomalous Andreev Conductance in InAs-AlSb Quantum Well Structures with Nb Electrodes, Phys. Rev. Lett. 1992; 69: 2847.

[6]   Zhang D, Wang J, DaSilva A M, Lee J S, Gutierrez H R, Chan M H W, Jain J, Samarth N, Superconducting Proximity Effect and Possible Evidence for Pearl Vortices in a Candidate Topological Insulator, Phys. Rev. B 2011; 84: 165120.

[7]   Williams J R, Bestwick A J, Gallagher P, Hong S S, Cui Y, Bleich A S, Analytis J G, Fisher I R, Goldhaber-Gordon D, Unconventional Josephson Effect in Hybrid Superconductor-Topological Insulator Devices, Phys. Rev. Lett. 2012; 109: 056803.

[8]   Qu F, Yang F, Shen J, Ding Y, Chen J, Ji Z, Liu G, Fan J, Jing X, Yang C, Lua L, Strong Superconducting Proximity Effect in Pb-Bi2Te3 Hybrid Structures, Sci Rep. 2012; 2: 339.

[9]   Heersche H B, Jarillo-Herrero P, Oostinga J B, Vandersypen L M K, Morpurgo A F, Bipolar Supercurrent in Graphene, Nature 2007; 446: 56–59.

[10] Morpurgo A F, Kong J, Marcus C M, Dai H, Gate-Controlled Superconducting Proximity Effect in Carbon Nanotubes, Science 1999; 286 (5438): 263–265.

[11] Jarillo-Herrero P, van Dam J A, Kouwenhoven L P, Quantum Supercurrent Transistors in Carbon Nanotubes, Nature 2006; 439: 953–956.

[12] Winkelmann C B, Roch N, Wernsdorfer W, Bouchiat V, Balestro F, Superconductivity in a Single-C60 Transistor, Nature Physics 2009; 5: 876–879.

[13] van Dam J A, Nazarov Y V, Bakkers E P A M, De Franceschi S, Kouwenhoven L P, Supercurrent Reversal in Quantum Dots, Nature 2006; 442: 667–670.

[14] Kasumov A Y, Kociak M, Guéron S, Reulet B, Volkov V T, Klinov D V, Bouchiat H, Proximity-Induced Superconductivity in DNA, Science 2001; 291 (5502): 280–282.

[15] Peña V, Sefrioui Z, Arias D, Leon C, Santamaria J, Varela M, Pennycook S J, Martinez J L, Coupling of Superconductors Through a Half-Metallic Ferromagnet: Evidence for a Long-Range Proximity Effect, Phys. Rev. B 2004; 69: 224502.

[16] Keizer R S, Goennenwein S T B, Klapwijk T M, Miao G X, Xiao G, Gupta A, A Spin Triplet Supercurrent Through the Half-Metallic Ferromagnet CrO2, Nature 2006; 439(7078): 825.

[17] Kitaev A Yu, Fault-Tolerant Quantum Computation by Anyons, Annals. Phys. 2003; 303(1): 2–30.

[18] Read N, Green D, Paired States of Fermions in Two Dimensions with Breaking of Parity and Time-Reversal Symmetries and the Fractional Quantum Hall Effect, Phys. Rev. B 2000; 61: 10267.

[19] Ivanov D A, Non-Abelian Statistics of Half-Quantum Vortices in p-Wave Superconductors, Phys. Rev. Lett. 2001; 86: 268.

[20] Das Sarma S, Nayak C, Tewari S, Proposal to Stabilize and Detect Half-Quantum Vortices in Strontium Ruthenate Thin Films: Non-Abelian Braiding Statistics of Vortices in a px+ipy Superconductor, Phys. Rev. B 2006; 73: 220502(R).

[21] Mackenzie A P, Maeno Y, The Superconductivity of Sr2RuO4 and the Physics of Spin-Triplet Pairing, Rev. Mod. Phys. 2003; 75: 657.

[22] Fu L, Kane C L, Superconducting Proximity Effect and Majorana Fermions at the Surface of a Topological Insulator, Phys. Rev. Lett. 2008; 10 (9): 096407.

[23] Sau J D, Lutchyn R M, Tewari S, Das Sarma S, Generic New Platform for Topological Quantum Computation Using Semiconductor Heterostructures, Phys. Rev. Lett. 2010; 104(4): 040502.

[24] Hasan M Z, Kane C L, Colloquium: Topological Insulators, Rev. Mod. Phys. 2010; 82: 3045.

[25] Fu L, Kane C L, Mele E J, Topological Insulators in Three Dimensions, Phys. Rev. Lett. 2007; 98: 106803.

[26] He L, Kou X, Wang K L, Review of 3D Topological Insulator Thin-Film Growth by Molecular Beam Epitaxy and Potential Applications, phys. stat. sol. - Rap. Res. Lett. 2013; 7: 50–63.

[27] Sasaki S, Kriener M, Segawa K, Yada K, Tanaka Y, Sato M, Ando Y, Topological Superconductivity in CuxBi2Se3

[28] Wang M X, Liu C, Xu J P, Yang F, Miao L, Yao M Y, Gao C L, Shen C, Ma X, Chen X, Xu Z A, Liu Y, Zhang S H, Qian D, Jia J F, Xue Q K, The Coexistence of Superconductivity and Topological Order in the Bi2Se3 Thin Films, Science 6 April 2012; 336: 52–55.

[29] Mourik V, Zuo K, Frolov S M, Plissard S R, Bakkers E P A M, Kouwenhoven L P, Signatures of Majorana Fermions in Hybrid Superconductor-Semiconductor Nanowire Devices, Science 2012; 336 (6084): 1003–1007.

[30] Deng M T, Yu C L, Huang G Y, Larsson M, Caroff P, Xu H Q, Anomalous Zero-Bias Conductance Peak in a Nb–InSb Nanowire–Nb Hybrid Device, Nano Lett. 2012; 12, 6414–6419.

[31] Das A, Ronen Y, Most Y, Oreg Y, Heiblum M, Shtrikman H, Zero-bias Peaks and Splitting in an Al-InAs Nanowire Topological Superconductor as a Signature of Majorana Fermions, Nature Physics 2012; 8: 887–895.

[32] Miao G X, Moodera J S, Spin Manipulation with Magnetic Semiconductor Barriers, Phys. Chem. Chem. Phys. 2014; DOI: 10.1039/c4cp04599h, in print.

[33] Alicea J, Majorana Fermions in a Tunable Semiconductor Device, Phys. Rev. B 2010; 81: 125318.

[34] Potter A C, Lee P A, Multichannel Generalization of Kitaev's Majorana End States and a Practical Route to Realize Them in Thin Films, Phys. Rev. Lett. 2010; 105: 227003.

[35] Law K T, Lee P A, Ng T K, Majorana Fermion Induced Resonant Andreev Reflection, Phys. Rev. Lett. 2009; 103: 237001.

[36] Kitaev A Y, Unpaired Majorana Fermions in Quantum Wires, Physics-Uspekhi 2001; 44: 131.

[37] Lutchyn R M, Sau J D, Das Sarma S Majorana Fermions and a Topological Phase Transition in Semiconductor-Superconductor Heterostructures. Phys. Rev. Lett. 2010; 105 (7): 077001.

[38] Oreg Y, Refael G, von Oppen F, Helical Liquids and Majorana Bound States in Quantum Wires, Phys. Rev. Lett. 2010; 105: 177002.

[39] Alicea J, Oreg Y, Refael G, von Oppen F, Fisher M P A, Non-Abelian Statistics and Topological Quantum Information Processing in 1D Wire Networks, Nature Physics 2011; 7: 412–417.

[40] Nadj-Perge S, Drozdov I K, Li J, Chen H, Jeon S, Seo J, MacDonald A H, Bernevig B A, Yazdani A, Observation of Majorana Fermions in Ferromagnetic Atomic Chains on a Superconductor, Science 2014; 346(6209): 602–607.

[41] Stanescu T D, Tewari S, Majorana Fermions in SemiconductorNanowires: Fundamentals, Modeling, and Experiment, J. Phys.: Condens. Matter 2013; 25: 233201.

[42] Beenakker C W J, Search for Majorana Fermions in Superconductors. Annu. Rev. Condens. Matter Phys. 2013; 4: 113.

[43] Lutchyn R M, Stanescu T D, Das Sarma S, Search for Majorana Fermions in Multiband Semiconducting Nanowires, Phys. Rev. Lett. 2011; 106: 127001.

[44] Buzdin A I, Proximity Effects in Superconductor-Ferromagnet Heterostructures, Rev. Mod. Phys. 2005; 77: 935–976.

[45] Bergeret F S, Volkov A F, Efetov K B, Odd Triplet Superconductivity and Related Phenomena in Superconductor-Ferromagnet Structures, Rev. Mod. Phys. 2005; 77: 1321–1373.

[46] Usadel K D, Generalized Diffusion Equation for Superconducting Alloys, Phys. Rev. Lett. 1970; 25: 507.

[47] Buzdin A I, Kuprianov M Y, Transition Temperature of a Superconductor-Ferromagnet Superlattice, Pis'ma Zh. Eksp. Teor. Fiz. 1990; 52, 1089–1091.

[48] Jiang J S, Davidović D, Reich D H, Chien C L, Oscillatory Superconducting Transition Temperature in Nb/Gd Multilayers, Phys. Rev. Lett. 1995; 74: 314.

[49] Mercaldo L V, Attanasio C, Coccorese C, Maritato L, Prischepa S L, Salvato M, Superconducting-Critical-Temperature Oscillations in Nb/CuMn Multilayers, Phys. Rev. B 1996; 53: 14040.

[50] Sidorenko A S, Zdravkov V I, Prepelitsa A A, Helbig C, Luo Y, Gsell S, Schreck M, Klimm S, Horn S, Tagirov L R, Tidecks R, Oscillations of the Critical Temperature in Superconducting Nb/Ni bilayers, Annalen der Physik 2003; 12: 37–50.

[51] Miao G X, Ramos A V, Moodera J S, Infinite Magnetoresistance from the Spin Dependent Proximity Effect in Symmetry Driven bcc-Fe/V/Fe Heteroepitaxial Superconducting Spin Valves,Phys. Rev. Lett. 2008; 101: 137001.

[52] Kontos T, Aprili M, Lesueur J, Grison X, Inhomogeneous Superconductivity Induced in a Ferromagnet by Proximity Effect, Phys. Rev. Lett. 2001; 86: 304.

[53] Tagirov L R, Low-Field Superconducting Spin Switch Based on a Superconductor/ Ferromagnet Multilayer, Phys. Rev. Lett. 1999; 83: 2058.

[54] Buzdin A I, Vedyayev A V, Ryzhanova N V, Spin-Orientation-Dependent Supercon‐ ductivity in F/S/F Structures, Europhys. Lett. 1999; 48: 686.

[55] Wolf S A, Kennedy J J, Nisenoff M, Properties of Superconducting rf Sputtered Ultra‐ thin Films of Nb, J. Vac. Sci. Technol. 1976; 13: 145.

[56] Tinkham M, Introduction to Superconductivity, McGraw-Hill, New York, 1978.

[57] Demler E A, Arnold G B, Beasley M R, Superconducting Proximity Effects in Mag‐ netic Metals, Phys. Rev. B 1997; 55: 15174.

[58] Berkowitz A E, Takano K, Exchange Anisotropy — A Review, J. Magn. Magn. Mater. 1999; 200: 552–570.

[59] Gu J Y, You C Y, Jiang J S, Pearson J, Bazaliy Ya B, Bader S D, Magnetization-Orienta‐ tion Dependence of the Superconducting Transition Temperature in the Ferromag‐ net-Superconductor-Ferromagnet System: CuNi/Nb/CuNi, Phys. Rev. Lett. 2002; 89: 267001.

[60] Potenza A, Marrows C H, Superconductor-Ferromagnet CuNi/Nb/CuNi Trilayers as Superconducting Spin-Valve Core Structures, Phys. Rev. B 2005; 71: 180503(R).

[61] Moraru I C, Pratt W P, Birge N O, Magnetization-Dependent Tc Shift in Ferromag‐ net/Superconductor/Ferromagnet Trilayers with a Strong Ferromagnet, Phys. Rev. Lett. 2006; 96: 037004.

[62] Nowak G, Zabel H, Westerholt K, Garifullin I, Marcellini M, Liebig A, Hjörvarsson B, Superconducting Spin Valves Based on Epitaxial Fe/V Superlattices, Phys. Rev. B 2008; 78: 134520.

[63] de Gennes P G, Coupling Between Ferromagnets Through a Superconducting Layer, Phys. Lett. 1966; 23: 10–11.

[64] Li B, Roschewsky N, Assaf B A, Eich M, Epstein-Martin M, Heiman D, Munzenberg M, Moodera J S, Superconducting Spin Switch with Infinite Magnetoresistance In‐ duced by an Internal Exchange Field, Phys. Rev. Lett. 2013; 110: 097001.

[65] Moodera J S, Hao X, Gibson G A, Meservey R, Electron-Spin Polarization in Tunnel Junctions in Zero Applied Field with Ferromagnetic EuS Barriers, Phys. Rev. Lett. 1988; 61: 637.

[66] Hao X, Moodera J S, Meservey R, Spin-Filter Effect of Ferromagnetic Europium Sul‐ fide Tunnel Barriers, Phys. Rev. B 1990; 42: 8235.